Refined Classical Force Field for Choline Chloride and Ethylene Glycol Mixtures over Wide Composition Range

Yong Zhang,[†] Henry Squire,[‡] Burcu Gurkan,[*,‡] and Edward J. Maginn[*,†]

[†]*Department of Chemical and Biomolecular Engineering, University of Notre Dame, Notre Dame, IN, USA*

[‡]*Department of Chemical and Biomolecular Engineering, Case Western Reserve University, Cleveland, Ohio 44106*

E-mail: beg23@case.edu; ed@nd.edu

Abstract

A classical force field based on the General Amber Force Field (GAFF) was refined for the simulation of choline chloride (ChCl) and ethylene glycol (EG) mixtures over a wide composition range by scaling the partial charges and van der Waals parameters. The scaling factors were derived by fitting the simulation results to only eight experimental density and viscosity data points of pure EG, and ChCl/EG mixtures at 1:2, 1:4, and 1:6 molar ratios. Using the refined force field, properties essential for electrochemical applications such as density, viscosity, self-diffusion coefficient, and ionic conductivity were calculated and excellent agreement to experimental results was found even for compositions and temperatures not used in the fitting procedure. In addition, new experimental data for density, viscosity, and ionic conductivity are reported as a function of temperature and composition for this mixture. To the best of our knowledge, this is the first classical force field developed for the study of ChCl/EG

mixtures over a composition range that includes the eutectic point. Using the new model, the liquid dynamics was studied in terms of ionic conductivity. It was found that the dynamics in ChCl/EG mixtures with ChCl mole fraction higher than 20% is similar to that of ionic liquids, high temperature molten salts and highly concentrated water-in-salt electrolytes.

Introduction

Deep eutectic solvents (DESs), particularly type III DESs,[1] have drawn extensive attention over the past two decades due to their potential for application in a wide variety of fields.[2–12] In addition to their favorable properties such as low volatility, low flammability, and electrochemical and thermal stability under common working conditions, DESs are highly tunable. Type III DESs are usually formed by mixing hydrogen bond acceptors (HBAs), such as halide salts, and hydrogen bond donors (HBDs), typically alcohols, amides, or carboxylic acids to form a liquid with a significantly depressed freezing point as compared to the parent components. By combining different HBAs and HBDs, there are potentially an unlimited number of DESs, before even considering mixtures of DESs or DESs with other additives.[13–15] Theoretically a DES could be tailored to serve any specific application and therefore DESs are usually considered "designer" solvents.

While the wide design space offers opportunities for designing solvents for particular applications, it has also created obstacles in developing fundamental structure-property understanding. Many efforts pursuing such understanding have been carried out using a variety of techniques in recent years.[9,13,16–25] However, few underlying principles are available to guide the design of a DES[26] and broad fundamental understanding of the link between composition, structure, and properties of DESs is still missing. For example, ethaline is one of the most studied DESs over the past decade, which is a 1:2 molar ratio mixture of choline chloride (ChCl) and ethylene glycol (EG). Crespo and co-workers recently studied the phase behavior of the ChCl and EG mixtures and found that the eutectic point is between 1:4 and

1:5 molar ratios instead of the commonly asserted value of 1:2.[27] Klein and co-workers also studied ChCl and EG mixtures reporting physical and electrochemical properties of 1:2, 1:4 and 1:6 ChCl:EG molar ratios.[28] It was found that the viscosity of the mixture decreases with increasing EG fraction, whereas the ionic conductivity shows a maximum at a ChCl:EG ratio of 1:4, suggesting that the 1:4 ratio mixture might be a better choice for electrochemical applications. These and other studies[13,19,29–31] clearly demonstrated the urgent need for systematic studies of DES mixtures over a wide composition range.

Classical molecular dynamics (CMD) simulations that utilize parameterized force fields to represent energetic interactions have proven to be a powerful tool to pursue such fundamental understanding. With CMD, one has the ability to calculate macroscopic thermodynamic and transport properties and simultaneously provide molecular level insights, something which is still a challenging task for ab initio MD (AIMD) simulations.[32,33] However, the reliability of such simulations highly depends on the accuracy of the applied force fields. Efforts have been made to develop accurate force fields for DES systems showing both successes and challenges. Ferreira and co-workers compared eight sets of parameters for ethaline, most of which are based on OPLS-AA force fields.[34] For the set with the best overall performance, the liquid density was significantly underestimated. Doherty and Acevedo tried to improve the OPLS-AA force field for eight choline chloride-based mixtures at 1:1, 1:2 or 1:3 HBA:HBD ratios, depending on the HBD, by fine-tuning the parameters against experimentally determined liquid structure and other bulk properties as well as first principle calculations.[35] The resultant force fields were able to reproduce experimental densities, viscosities, heat capacities, and surface tensions quite well. However, the simulated dynamics of the liquids are similar to supercooled liquids at and slightly higher than room temperature. As a result, the models were unable to capture the experimental self-diffusion coefficients under ambient conditions. Another popular force field for liquid simulation is the general Amber force field (GAFF).[36] By introducing a weak van der Waals (vdW) term to the hydroxyl hydrogen atoms to better capture the hydrogen bonding behavior,[37] Perkins and co-workers showed that GAFF can

describe ethaline and two other DESs reasonably well when the partial charges derived using the RESP method[38] following a multiconformation procedure were scaled by 0.9.[39] Although not perfect as we tested on ChCl and EG mixture at 1:2 ratio,[33] this is one of the successful developments in simulating ethaline. Also based on GAFF, Chaumont and co-workers took an alternative route to improve the force field performance.[40] Without scaling the partial charges, the authors developed force fields for ethaline and glyceline (1:2 molar ratio mixture of ChCl and glycerol) by tuning the vdW parameters of the oxygen and hydrogen atoms of the hydroxyl groups. This force field was accurate in predicting the static, dynamical, and structural properties of both DESs. Other force fields have also been reported for DES systems in the literature.[41–44] However, most of these models focus on one fixed HBA and HBD ratio, which, as shown in the current work, could limit their applications to other compositions.

In the current work, the non-bonded parameters in the GAFF force field for ChCl and EG mixtures were tuned against recently published experimental density and viscosity data at 298 K over a wide ChCl fraction. Using the refined model, the experimental density, viscosity, ionic conductivity, and self-diffusion coefficients as functions of temperature and ChCl fraction were reproduced quantitatively.

MD simulations

CMD simulations were carried out using the package LAMMPS.[45] The long-range electrostatic interactions were calculated using the particle-particle particle-mesh (PPPM) method[46] with a real space cutoff of 12 Å. The same cutoff was used for van der Waals interactions and a tail correction[47] was applied.

The simulation boxes at different ChCl:EG ratios were built up by placing the proper numbers (see Table 1) of Ch^+, Cl^-, and EG molecules randomly in a cubic box using the package Packmol.[48,49] Each system was equilibrated for 2 ns in the isothermal-isobaric (NPT)

ensemble followed by production simulations in the canonical ensemble (NVT). The Nosé-Hoover thermostat with chain length of three was used to control the temperature[50] and an extended Lagrangian approach[51] was used to control the pressure. A time constant of 100 fs was used for both the thermostat and barostat. The pressure was fixed at one atmosphere in all constant pressure simulations with isotropic volume fluctuations. Periodic boundary conditions were applied in all directions and a time step of 1 fs was used in all simulations.

The viscosity was calculated using the Green-Kubo relation

$$\eta = \frac{V}{6k_BT}\sum_{\alpha\leq\beta}\int_0^\infty \langle \bar{P}_{\alpha\beta}(t)\cdot\bar{P}_{\alpha\beta}(0)\rangle \, \mathrm{d}t \tag{1}$$

where V is the system volume, k_B is the Boltzmann constant, T is temperature, and $\bar{P}_{\alpha\beta}$ denotes an element $\alpha\beta$ of a modified pressure tensor as detailed in our previous publication.[33] The time-decomposition procedure[52] was used in the calculation, in which 30 independent equilibrium NVT simulations, up to 10 ns each, were carried out for each data point. The uncertainty was estimated using a bootstrap method.[53]

The ionic conductivity was calculated using the Einstein relation

$$\sigma_E = \frac{1}{6k_BTV}\lim_{t\to\infty}\frac{d}{dt}\left\langle\sum_{i=1}^{N_{ion}}\sum_{j=1}^{N_{ion}} q_iq_j[\mathbf{r_i}(\mathbf{t})-\mathbf{r_i}(\mathbf{0})]\cdot[\mathbf{r_j}(\mathbf{t})-\mathbf{r_j}(\mathbf{0})]\right\rangle \tag{2}$$

where $\mathbf{r}_i(t)$ is the center of mass (COM) position of species i at time t, and N_{ion} is the total number of Ch^+ and Cl^- ions in the mixtures. To improve the statistics in the Einstein

Table 1: Composition of simulation boxes.

ChCl:EG	Number of ChCl	Number of EG
1:2	250	500
1:3	200	600
1:4	175	700
1:5	150	750
1:6	125	750
pure EG	-	1000

relation calculation, a procedure similar to the time-decomposition method for viscosity[52] was applied. For each system, 30 independent trajectories were generated in the NVT ensemble. Eq 2 was applied to each trajectory, and the average over 30 trajectories was reported. The uncertainty was estimated using the bootstrap method.[53] A finite system size correction was applied to the self ($i = j$ in Eq 2) terms using the method proposed by Yeh and Hummer[54,55] with the calculated viscosities.

The self-diffusion coefficient was calculated using the Einstein relation

$$D = \frac{1}{6} \lim_{t\to\infty} \frac{d}{dt} \frac{1}{N} \sum_{i=1}^{N} \left\langle |\mathbf{r}_i(t) - \mathbf{r}_i(0)|^2 \right\rangle \tag{3}$$

where N is the number of individual species. The effect of finite system size was corrected using the Yeh and Hummer method[54,55] with the calculated viscosity.

Force Field Development

As mentioned in the Introduction, the model based on GAFF developed by Perkins and co-workers[39] has been one of the most successful force fields for ethaline. Therefore, instead of starting from the original GAFF, we took Perkins model as the base for further refinement. To limit the number of the tuning parameters, a scaling factor was applied to charge, q, and vdW parameters, σ and ϵ, respectively, for each molecule or ion. This yields three scaling factors for EG (S_q^{EG}, S_σ^{EG} and S_ϵ^{EG}) and five scaling factors for Ch^+ and Cl^- ions (S_q^{ChCl}, S_σ^{Ch}, S_ϵ^{Ch}, S_σ^{Cl} and S_ϵ^{Cl}). To fit these scaling factors, a two-step procedure was applied. In the first step, S_q^{EG}, S_σ^{EG} and S_ϵ^{EG} were derived by fitting to experimental results of pure EG. The scaling factors for Ch^+ and Cl^- ions were then derived in the second step with the scaling factor of pure EG from the first step unchanged.

Pure EG

The scaling factors S_q^{EG}, S_σ^{EG} and S_ϵ^{EG} were derived by fitting three experimental properties of the pure EG: density (ρ) at 298 K, the slope of the density vs temperature ($d\rho/dT$)

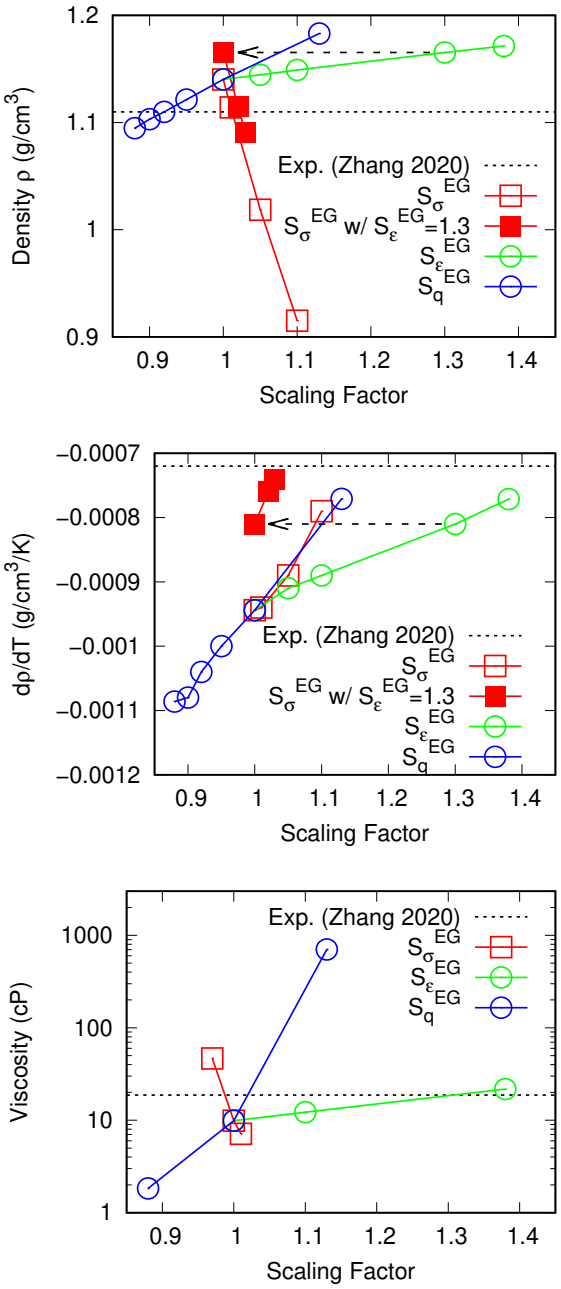

Figure 1: Calculated density (ρ) at 298 K, density∼T slope ($d\rho/dT$), and viscosity at 298 K as a function of scaling factors S_q^{EG}, S_σ^{EG} and S_ϵ^{EG} for pure EG. Experimental values (Zhang 2020[33]) are shown in dotted lines.

between 298 and 363 K, and the viscosity (η) at 298 K. The effect of each scaling factor on the three properties was checked by adjusting each scaling factor separately. The results are shown in Figure 1. Both ρ and $d\rho/dT$ scale linearly with all three scaling factors and the trends agree with common intuition. For example, the density ρ increases with increasing S_ϵ^{EG} and S_q^{EG} because of the stronger intermolecular interactions. Density decreases with increasing S_σ^{EG} because larger atomic diameters push molecules farther away from each other, therefore lowering density. With $S_\epsilon^{EG} = 1.3$, simulations were carried out for a few values of S_σ^{EG}. As shown in the plots, the same linear behavior was observed for both ρ and $d\rho/dT$. Viscosity is much more expensive to compute than density, so only three values of each

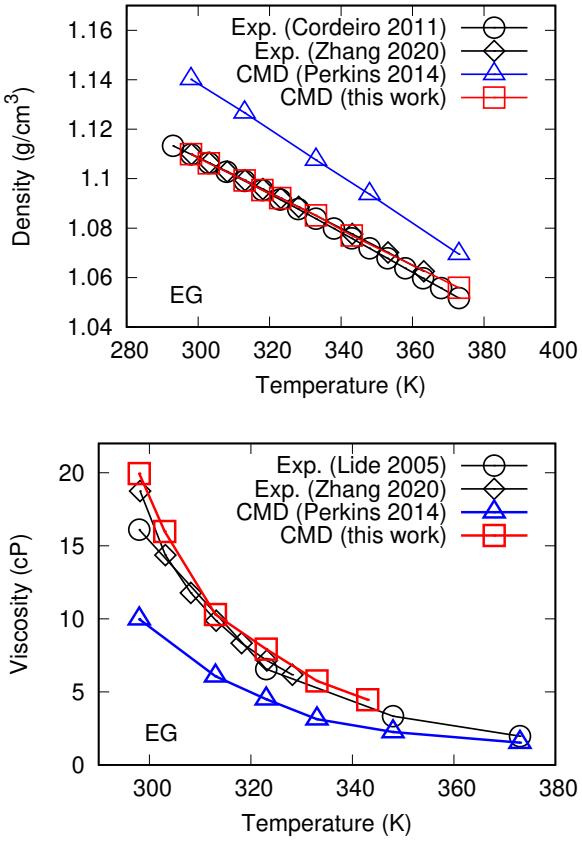

Figure 2: Calculated density and viscosity as a function of temperature for pure EG and compared to experimental results (Cordeiro 2011,[24] Zhang 2020,[33] and Lide 2005[56]). The estimated uncertainty in the calculated results are smaller than the size of the symbols. The results calculated in the current work using a previous force field[39] are also included for comparison.

scaling factor were tested against viscosity. As shown in Figure 1, when viscosity is plotted on a logarithmic scale, nearly linear relationships were observed for all three scaling factors, with S_q^{EG} deviating the most from linearity. These results suggest that the three properties can be predicted to scale linearly with all three scaling factors as well as the combinations of the scaling factors. Therefore, instead of trial and error sampling in the three dimensional parameter space, which would require a large number of simulations, the determination of the three scaling factors was achieved by solving three linear equations with three variables. With minor manual adjustment, the final set of the scaling factors for pure EG was found to be $S_q^{EG} = 1.046$, $S_\sigma^{EG} = 1.028$, and $S_\epsilon^{EG} = 1.340$. With these scaling factors, the density and viscosity of pure EG as a function of temperature were calculated and the results are shown in Figure 2. The results using the Perkins model[39] are also included. The accuracy of the calculation was significantly improved with the new model, and both density and viscosity agree with experimental values[33,57] very well over the entire temperature range, although only one viscosity value at 298 K was used in the fitting. This new model of EG with the optimized scaling factors was used in the fitting of scaling factors for Ch^+ and Cl^-.

ChCl and EG Mixtures

The five scaling factors S_q^{ChCl}, S_σ^{Ch}, S_ϵ^{Ch}, S_σ^{Cl} and S_ϵ^{Cl} for Ch^+ and Cl^- ions were fit to reproduce five experimental values at 298 K, the densities at ChCl:EG ratios of 1:2 and 1:4, and the viscosities at ChCl:EG ratios of 1:2, 1:4 and 1:6. Ionic conductivity was not included in the fitting, but it was calculated for each set of the scaling factors from the same simulations for the viscosity calculation. The effect of each scaling factor on the calculated properties was also studied. However, unlike the cases for pure EG, some correlations show large deviations from linear behavior. The trends are more complicated than those of pure EG as well. Some trends are even against common intuition. For example, with increasing S_σ^{Ch}, the liquid density was found to decrease, as expected, but the calculated viscosity was found to increase and the ionic conductivity decreases for all three compositions. A

possible reason for this abnormal behavior lies in the complicated interactions existing in these mixtures. As we pointed out previously,[33] EG-Cl^- interactions are stronger than

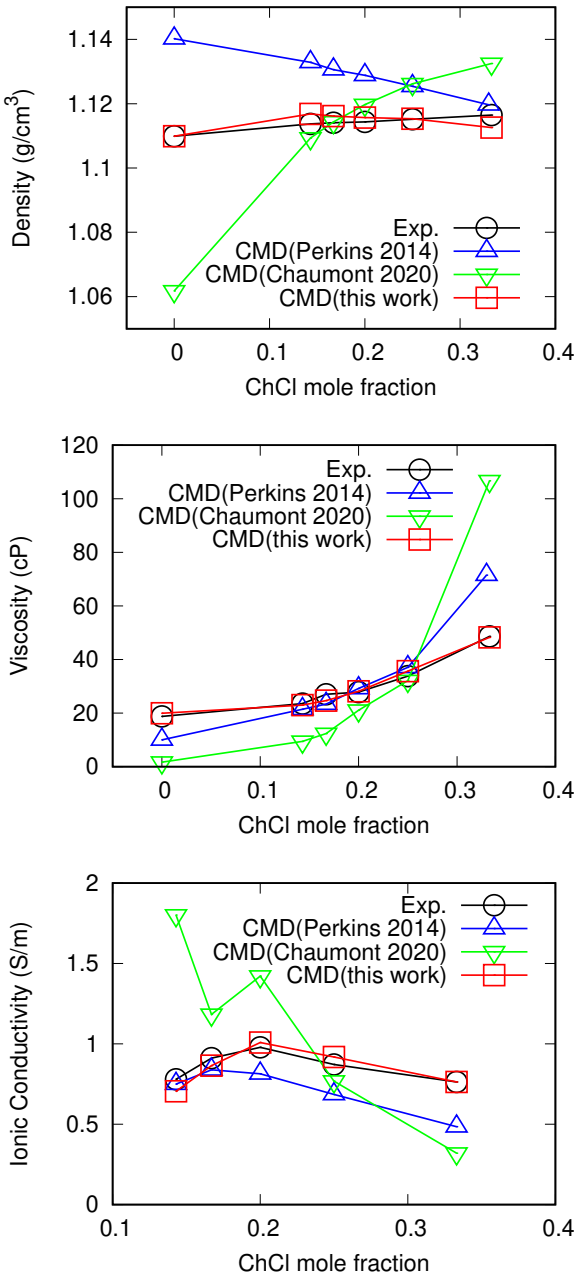

Figure 3: Calculated density, viscosity and ionic conductivity for ChCl and EG mixtures as a function of ChCl fraction at 298K and compared to experimental results.[28] The estimated uncertainty in the calculated results are smaller than the size of the symbols therefore not shown. The results calculated in the current work using previous force fields (Perkins 2014[39] and Chaumont 2020[40]) were also included for comparison.

other interactions in ethaline. When σ is increased for Ch^+ atoms, Ch^+-Cl^- and Ch^+-EG interactions become weaker. As a result, EG-Cl^- interactions could be enhanced due to the increased coordination between them and cause the increase in viscosity and decrease in ionic conductivity.

Five linear functions were solved to get the initial set of scaling factors, similar to the case of pure EG. However, significant deviations were observed from linear correlation between the calculated properties and the scaling factors. Therefore, further manual adjustments were made to improve the performance of the force field initially derived from the linear functions. During this process, values of the calculated ionic conductivity were also considered, although they were not fit to experimental results directly. Approximately 40 sets of scaling factors were tested. The scaling factors with the best overall performance are $S_q^{ChCl} = 0.833$, S_σ^{Ch} =0.880, S_ϵ^{Ch}=1.429, $S_\sigma^{Cl} = 1.107$, and $S_\epsilon^{Cl} = 0.502$. Note that the scaling factor $S_q^{ChCl} = 0.833$ is relative to a full charge of 1.0. Therefore in the refined force field, the total charges on Ch^+ and Cl^- are $\pm$0.833 e, respectively, slightly lower than the 0.9 e charge in the Perkins model.[39]

The calculated density, viscosity, and ionic conductivity as a function of ChCl fraction using this force field are shown in Figure 3 and compared with experimental results. We report new experimental data in the figures, which are listed in Table S2. The calculated results using two previous force field models[39,40] are also included. For all three properties, previous models generally behave poorly although the results at certain compositions can be accurate. For the results using the new model, the slope of density with respect to ChCl fraction varies from experiment slightly. However, considering the small range of the density over the composition range and the fact that the largest deviation from experiment is only -0.003 g/cm^3 or -0.3% at a ChCl:EG ratio of 1:2, the agreement between the calculated density and experimental data is very good. In addition, the agreement between the calculated and experimentally measured viscosity and ionic conductivity over the whole composition range is nearly perfect. The maximum ionic conductivity at ChCl:EG=1:4 (ChCl mol% = 20%)

as determined by experiment is also successfully captured. Overall, the performance of the new model was found to be excellent, despite the fact that it was fit to only two density and three viscosity data points at three compositions. The refined non-bonded parameters for EG and ChCl are provided in Table S1 in the Supporting Information (SI).

Results and Discussion

The refined model was further validated by comparing the calculated results to available experiments beyond the fitting properties or conditions. Figure 4 shows the calculated self-diffusion coefficients of the mixture with ChCl:EG=1:2 ratio as a function of temperature. The results using Perkins' model[39] are also included. Both models correctly capture the trend that the self-diffusivity increases with increasing temperature and the order of the self-diffusivity is EG $>$ Cl^- $>$ Ch^+. The new model is more accurate than the previous model, although self-diffusivity was not explicitly included in the fitting procedure.

As mentioned earlier, the new model of the ChCl and EG mixture was derived by fitting to experimental data at 298 K. The performance of the new model at other temperatures was checked at different ChCl:EG ratios. The calculated density, viscosity, and ionic conductivity are shown in Figure 5 for ChCl:EG=1:2 and 1:4 ratios. The results for ChCl:EG=1:3, 1:5, and 1:6 ratios are provided in Figures S1 to S3 in the SI. The calculated results agree with experimental data very well at all temperatures, especially at low ChCl fractions. This suggests that the refined model is able to properly capture the temperature dependence beyond the fitting temperature. Numerical results at all compositions are summarized in Tables S3 to S5 in the SI.

A recent experimental study showed that the ChCl:EG=1:4 mixture has higher ionic conductivity than other compositions.[28] Using the new model, the ionic conductivity in the ChCl and EG mixtures was studied in greater detail. In addition to the Einstein relation (Eq. 2), the ionic conductivity can also be calculated based on the self-diffusion coefficients

using the Nernst-Einstein (NE) relation

$$\sigma_{NE} = \frac{N_{ChCl}}{V k_B T}(q^2_{Ch^+} D_{Ch^+} + q^2_{Cl^-} D_{Cl^-}) \tag{4}$$

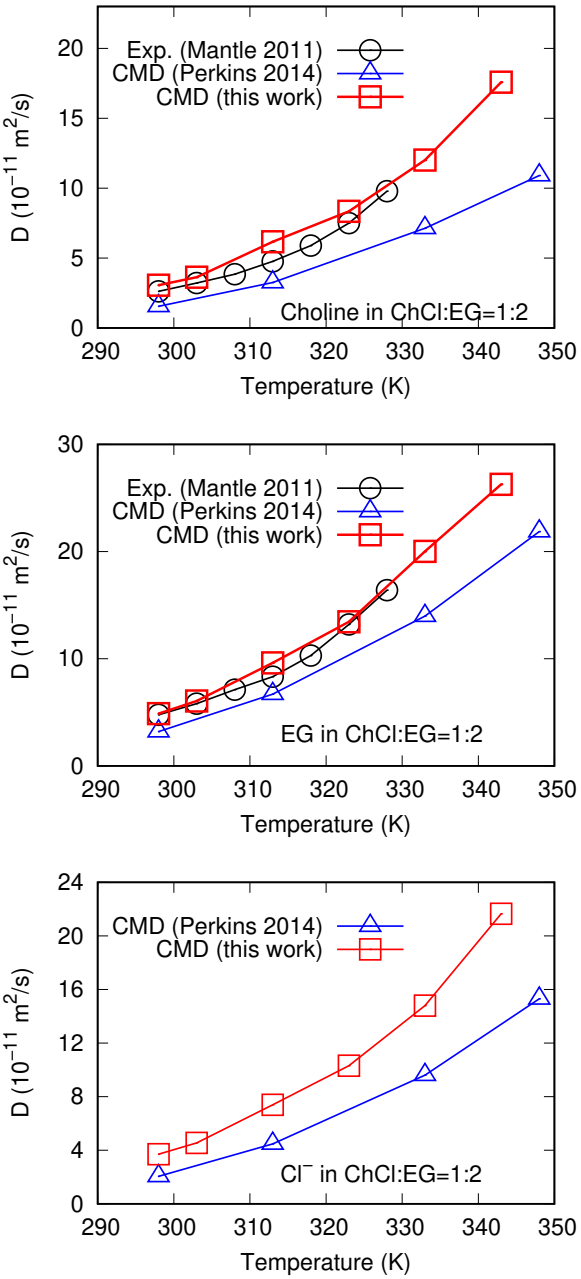

Figure 4: Calculated self-diffusion coefficients in ChCl:EG=1:2 mixture at 298K and compared to available experimental results.[58] The results calculated in the current work using previous force field[39] are also included for comparison.

where N_{ChCl} is the number of ChCl ion pairs in a given volume V, q_{Ch^+} and q_{Cl^-} are the total charges on the cation and anion, and D_{Ch^+} and D_{Cl^-} are the self-diffusivities of the cation and anion, respectively. The results at 298 K are shown in Figure 6(a). The results calculated using the Einstein relation (Eq. 2) are also included for comparison. As Eq 4

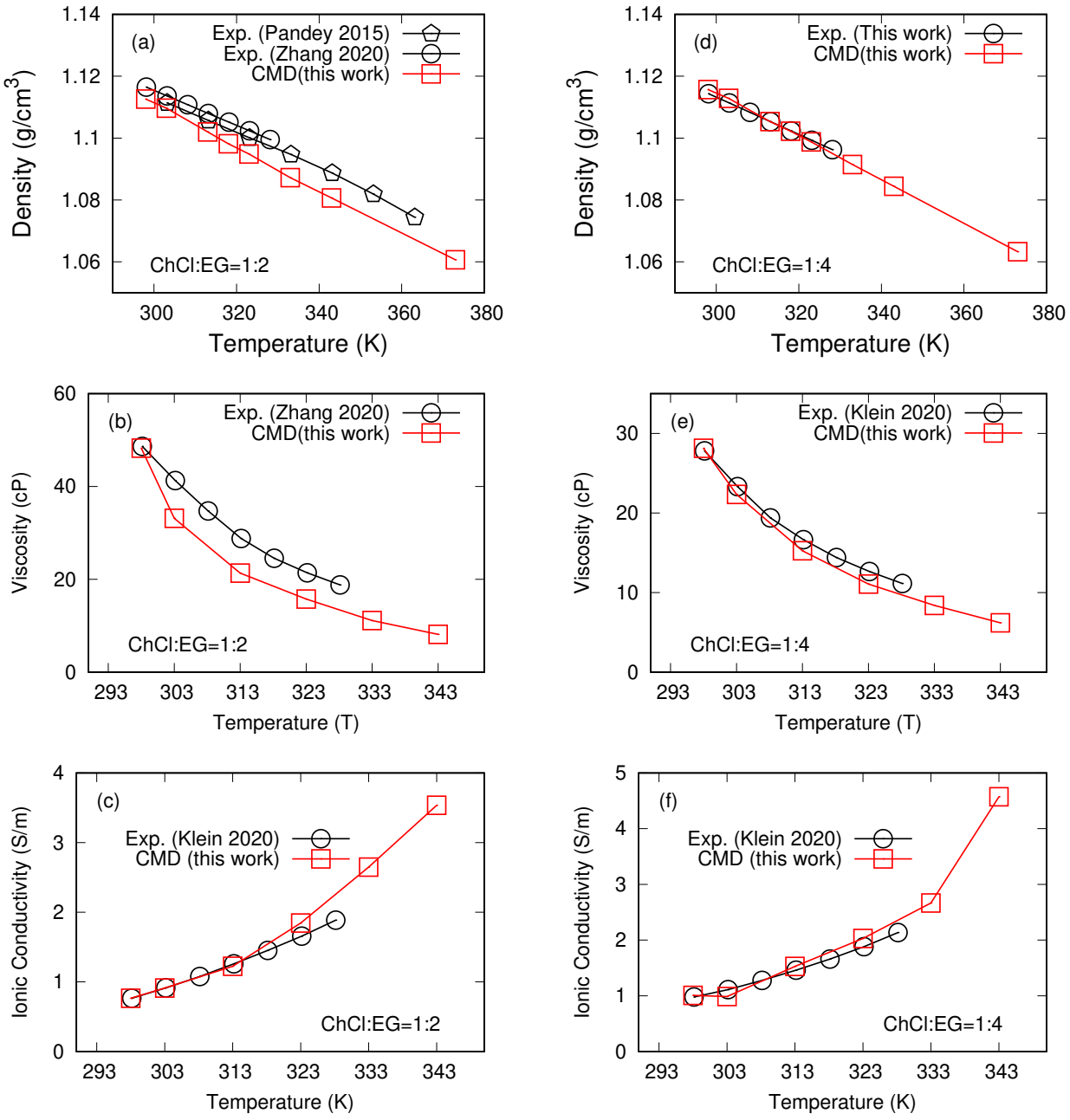

Figure 5: Calculated density, viscosity, and ionic conductivity as a function of temperature for ChCl:EG=1:2 and ChCl:EG=1:4 mixtures using the new force field and compared to experimental results.[28]

indicates, the NE relation assumes no correlation between the ions, which is usually valid only for dilute solutions. Such correlations between the ions are considered in Eq. 2. As shown in the figure, compared to the Einstein relation, the NE relation tends to overestimate the ionic conductivity at all compositions. The ratio σ_E/σ_{NE}, which is known as the ionicity or the inverse Haven ratio, is a measure of the extent of ion dissociation in the solution. The calculated inverse Haven ratios are included in Figure 6, which show that, in addition to σ_E, the inverse Haven ratio also shows a maximum at 1:4 ChCl:EG ratio.

An alternative way to understand the correlations between ions is based on Eq 2. In Eq 2, by considering i=j for both Ch^+ and Cl^- (σ_{Ch} and σ_{Cl}), i≠j for the same species (σ_{Ch-Ch} and σ_{Cl-Cl}) and different species (σ_{Ch-Cl}), the correlation between ions and the corresponding contributions to the overall ionic conductivity can be quantified. The calculated results are shown in Figure 6(b). Note that the sum of the self terms is equivalent to the results using the Nernst-Einstein relation $\sigma_{NE} = \sigma_{Ch} + \sigma_{Cl}$. As shown in the figure, both σ_{Ch} and σ_{Cl} are positive at all compositions and a maximum is observed at a ChCl mole fraction of 20% (ChCl:EG=1:4), similar to the behavior in the overall ionic conductivity σ_E. Due to the slower diffusivity of Ch^+ relative to that of Cl^-, the Ch^+ self contribution σ_{Ch} is much smaller than that of the Cl^- self term σ_{Cl}. For the terms corresponding to the same species but distinct ions σ_{Ch-Ch} and σ_{Cl-Cl}, both make negative contributions to σ_E at

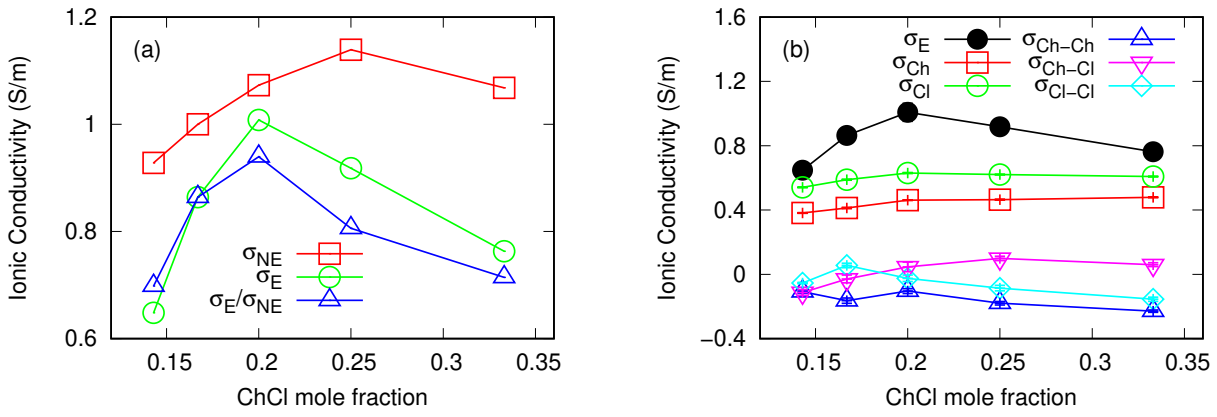

Figure 6: Calculated ionic conductivity and inverse Haven ratio (a) and contributions from each interaction (b) as a function of ChCl fraction using the new force field at 298 K.

ChCl mole fractions 20% or higher due to the repulsion between ions with like charges, whereas the values are close to zero at low ChCl fractions. Except for the two low ChCl mole fraction solutions, the cross term σ_{Ch-Cl} makes a positive contribution to the overall ionic conductivity. This result suggests that the dynamics in these mixtures at 20% and higher ChCl mole fraction share similarities with ionic liquids and high temperature molten salts,[59,60] which are completely composed of ionic species, and water-in-salt electrolytes (WISE), which are highly concentrated salt aqueous solutions.[61]

Conclusions

Based on force field parameters proposed previously,[39] the GAFF force field was refined for ChCl and EG mixtures by scaling the atomic partial charges and vdW parameters to fit experimental density and viscosity at multiple compositions. The scaling factors were derived for pure EG first by fitting the calculated results to experimental density and viscosity at 298 K, and experimental density dependence on temperature. This refined EG model was fixed when the scaling factors for ChCl were derived in the next step. To fit the scaling factors for Ch^+ and Cl^-, five experimental data points at 298 K, two densities and three viscosities, respectively, were considered. The performance of the refined force field is significantly improved compared to the original model and the calculated density, viscosity, self-diffusion coefficient, and ionic conductivity agree with experiments quantitatively even beyond the fitting compositions and temperatures. Using the new model, the ionic conductivity of the ChCl and EG mixtures as a function of ChCl mole fraction was studied. It was found that the dynamics in these mixtures with ChCl mole fraction equal to or greater than 20% are similar to that of ionic liquids, high temperature molten salts, and highly concentrated water-in-salt electrolytes.

The refined model makes it possible to systematically study the liquid properties of the ChCl and EG mixtures as a function of ChCl fraction over a wide composition range. To

the best of our knowledge, this is the first time that a classical force field was specifically developed for a DES over a wide HBA:HBD ratio. However, it is challenging for a force field to work for all properties, especially for liquid as complicated as DES. In the current work, special attention was paid to properties that are important for electrochemical applications. However, the refined force field could be useful for determining other properties as well. In addition, the procedure used in the current work to refine the ChCl and EG force field can be easily applied to other DES or liquid mixture systems.

Supporting Information Available

Experimental methods; refined non-bonded parameters for Ch^+, Cl−, and EG; experimental density, viscosity and ionic conductivity at ChCl:EG=1:3, 1:4 and 1:5 ratios; calculated density, viscosity, and ionic conductivity at all ChCl and EG compositions using the refined force fields.

Acknowledgement

This work was funded by Breakthrough Electrolytes for Energy Storage (BEES) - an Energy Frontier Research Center funded by the U.S. Department of Energy, Office of Science, Basic Energy Science under award number DE-SC0019409. We thank the Center for Research Computing (CRC) at the University of Notre Dame for providing computational resources.

Literature Cited

(1) Smith, E. L.; Abbott, A. P.; Ryder, K. S. Deep eutectic solvents (DESs) and their applications. *Chem. Rev.* **2014**, *114*, 11060–11082.

(2) Nkuku, C. A.; LeSuer, R. J. Electrochemistry in Deep Eutectic Solvents. *J. Phys. Chem. B* **2007**, *111*, 13271–13277.

(3) Singh, B.; Lobo, H.; Shankarling, G. Selective N-Alkylation of Aromatic Primary Amines Catalyzed by Bio-catalyst or Deep Eutectic Solvent. *Cat. Lett.* **2011**, *141*, 178–182.

(4) Carriazo, D.; Serrano, M. C.; Gutierrez, M. C.; Ferrer, M. L.; del Monte, F. Deep-eutectic solvents playing multiple roles in the synthesis of polymers and related materials. *Chem. Soc. Rev.* **2012**, *41*, 4996–5014.

(5) Li, C.; Li, D.; Zou, S.; Li, Z.; Yin, J.; Wang, A.; Cui, Y.; Yao, Z.; Zhao, Q. Extraction desulfurization process of fuels with ammonium-based deep eutectic solvents. *Green Chem.* **2013**, *15*, 2793–2799.

(6) Shen, D.; Vukmirovic, M. B.; Akolkar, R. Understanding the role of complexation in the charge-transfer kinetics of the Cu^{2+} + e $\leftrightarrow$ Cu^{+} redox reaction in Ethaline deep eutectic solvent. *J. Electrochem. Soc.* **2019**, *166*, E526–E532.

(7) Hallett, J. E.; Hayler, H. J.; Perkin, S. Nanolubrication in deep eutectic solvents. *Phys. Chem. Chem. Phys.* **2020**, *22*, 20253–20264.

(8) Shishov, A.; Pochivalov, A.; Nugbienyo, L.; Andruch, V. Deep eutectic solvents are not only effective extractants. *Trends Analyt. Chem.* **2020**, *129*, 115956.

(9) Hansen, B. B. et al. Deep eutectic solvents: A review of fundamentals and applications. *Chem. Rev.* **2021**, *121*, 1232–1285.

(10) Plotka-Wasylka, J.; Rutkowska, M.; de la Guardia, M. Are deep eutectic solvents useful in chromatography? A short review. *J. Chromatogr. A* **2021**, *1639*, 461918.

(11) Chandran, K.; Kait, C. F.; Wilfred, C. D.; Zaid, H. F. M. A review on deep eutectic solvents: Physiochemical properties and its application as an absorbent for sulfur dioxide. *J. Mol. Liq.* **2021**, *338*, 117021.

(12) Pietro, M. E. D.; Mele, A. Deep eutectics and analogues as electrolytes in batteries. *J. Mol. Liq.* **2021**, *338*, 116597.

(13) Percevault, L.; Jani, A.; Sohier, T.; Noirez, L.; Paquin, L.; Gauffre, F.; Morineau, D. Do deep eutectic solvents form uniform mixtures beyond molecular microheterogeneities? *J. Phys. Chem. B* **2020**, *124*, 9126–9135.

(14) Alfurayj, I.; Fraenza, C. C.; Zhang, Y.; Pandian, R.; Spittle, S.; Hansen, B.; Dean, W.; Gurkan, B.; Savinell, R.; Greenbaum, S.; Maginn, E.; Sangoro, J.; Burda, C. Solvation dynamics of wet ethaline: Water is the magic component. *J. Phys. Chem. B* **2021**, *125*, 8888–8901.

(15) Chroma, R.; Vilkova, M.; Shepa, I.; Makos-Chelstowska, P.; Andruch, V. Investigation of tetrabutylammonium bromide-glycerol-based deep eutectic solvents and their mixtures with water by spectroscopic techniques. *J. Mol. Liq.* **2021**, *330*, 115617.

(16) Ibrahim, T. H.; Sabri, M. A.; Jabbar, N. A.; Nancarrow, P.; Mjalli, F. S.; AlNashef, I. Thermal conductivities of choline chloride-based deep eutectic solvents and their mixtures with water: Measurement and estimation. *Molecules* **2020**, *25*, 3816.

(17) Kaur, S.; Kumari, M.; Kashyap, H. K. Microstructure of deep eutectic solvents: current understanding and challenges. *J. Phys. Chem. B* **2020**, *124*, 10601–10616.

(18) Shayestehpour, O.; Zahn, S. Molecular features of reline and homologous deep eutectic solvents contributing to nonideal mixing behavior. *J. Phys. Chem. B* **2020**, *124*, 7586–7597.

(19) Bonomo, M.; Gontrani, L.; Capocefalo, A.; Sarra, A.; Nucara, A.; Carbone, M.; Postorino, P.; Nidi, D. A combined electrochemical, infrared and EDXD tool to disclose deep eutectic solvents formation when one precursor is liquid: Glyceline as case study. *J. Mol. Liq.* **2020**, *319*, 114292.

(20) Wang, Y.; Chen, W.; Zhao, Q.; Jin, G.; Xue, Z.; Wang, Y.; Mu, T. Ionicity of deep eutectic solvents by Walden plot and pulsed field gradient nuclear magnetic resonance (PFG-NMR). *Phys. Chem. Chem. Phys.* **2020**, *22*, 25760–25768.

(21) Aryafard, M.; Karimi, A.; Reza, A.; Harifi-Mood,; Minofar, B. Molecular dynamics simulations, solvatochromic parameters, and preferential solvation in aqueous solutions of ethaline, ethylene glycol, and choline chloride. *J. Chem. Eng. Data* **2020**, *65*, 4556–4566.

(22) Rajbangshi, J.; Mukherjee, K.; Biswas, R. Heterogeneous orientational relaxations and translation-rotation decoupling in (choline chloride + urea) deep eutectic solvents: Investigation through molecular dynamics simulations and dielectric relxation measurements. *J. Phys. Chem. B* **2021**, *125*, 5920–5936.

(23) Jani, A.; Malfait, B.; Morineau, D. On the coupling between ionic conduction and dipolar relaxation in deep eutectic solvents: Influence of hydration and glassy dynamics. *J. Chem. Phys.* **2021**, *154*, 164508.

(24) Ferreira, E. S.; Voroshylova, L. V.; Figueiredo, N. M.; Cordeiro, M. M. D. Molecular dynamic study of alcohol-based deep eutectic solvents. *J. Chem. Phys.* **2021**, *155*, 064506.

(25) Rain, M. I.; Iqbal, H.; Saha, M.; Ali, M. A.; Chohan, H. K.; Rahman, M. S.; Halim, M. A. A comprehensive computational and principal component analysis on various choline chloride-based deep eutectic solvents to reveal their structural and spectroscopic properties. *J. Chem. Phys.* **2021**, *155*, 044308.

(26) Gurkan, B.; Squire, H.; Pentzer, E. Metal-Free Deep Eutectic Solvents: Preparation, Physical Properties, and Significance. *Journal of Physical Chemistry Letters* **2019**, *10*, 7956–7964.

(27) Crespo, E. A.; Silva, L. P.; Lloret, J. O.; Carvalho, P. J.; lourdes F. Vega,; Llovell, F.; Coutinho, J. A. A methodology to parameterize SAFT-type equations of state for solid precursors of deep eutectic solvents: the example of cholinium chloride. *Phys. Chem. Chem. Phys.* **2019**, *21*, 15046–15061.

(28) Klein, J. M.; Squire, H.; Dean, W.; Gurkan, B. E. From salt in solution to solely ions: Solvation of methyl viologen in deep eutectic solvents and ionic liquids. *J. Phys. Chem. B* **2020**, *124*, 6348–6357.

(29) Alizadeh, V.; Malberg, F.; Padua, A. A.; Kirchner, B. Are there magic compositions in deep eutectic solvents? Effects of composition and water content in choline chloride/ethylene glycol from ab initio molecular dynamics. *J. Phys. Chem. B* **2020**, *124*, 7433–7443.

(30) Abranches, D. O.; Silva, L. P.; Martins, M. A.; Coutinho, J. A. Differences on the impact of water on the deep eutectic solvents betaine/urea and choline/urea. *J. Chem. Phys.* **2021**, *155*, 034501.

(31) Alhadid, A.; Mokrushina, L.; Minceva, M. Influence of he molecular structure of constituents and liquid phase non-ideality on the viscosity of deep eutectic solvents. *Molecules* **2021**, *26*, 4208.

(32) de Gastilla, A. G.; Bittner, J. P.; Muller, S.; Jakobtorweihen, S. Thermodynamic and transport properties modeling of deep eutectic solvents: A review on g^E-models, equations of state, and molecular dynamics. *J. Chem. Eng. Data* **2020**, *65*, 943–967.

(33) Zhang, Y.; Poe, D.; Heroux, L.; Squire, H.; Doherty, B. W.; Long, Z.; Dadmun, M.; gurkan, B.; Tuckerman, M. E.; Maginn, E. J. Liquid structure and transport properties of the deep eutectic solvent ethaline. *J. Phys. Chem. B* **2020**, *124*, 5251–5264.

(34) Ferreira, E. S.; Voroshylova, I. V.; Pereira, C. M.; Cordeiro, M. N. D. Improved force

field model for the deep eutectic solvent ethaline: Reliable physicochemical properties. *J. Phys. Chem. B* **2016**, *120*, 10124–10137.

(35) Doherty, B.; Acevedo, O. OPLS force field for choline chloride-based deep eutectic solvents. *J. Phys. Chem. B* **2018**, *122*, 9982–9993.

(36) Wang, J.; Wolf, R. M.; Caldwell, J. W.; Kollman, P. A.; Case, D. A. Development and Testing of a General Amber Force Field. *J. Comput. Chem.* **2004**, *25*, 1157–1174.

(37) Liu, H.; Maginn, E.; Visser, A. E.; Bridges, N. J.; Fox, E. B. Thermal and transport properties of six ionic liquids: An experimental and molecular dynamics study. *Ind. Eng. Chem. Res.* **2012**, *51*, 7242–7254.

(38) Bayly, C.; Cieplak, P.; Cornell, W. D.; Kollman, P. A. A Well-behaved Electrostatic Potential Based Method Using Charge Restraints for Deriving Atomic Charges: the RESP Model. *J. Phys. Chem.* **1993**, *97*, 10269–10280.

(39) Perkins, S. L.; Painter, P.; Colina, C. M. Experimental and computational studies of choline chloride-based deep eutectic solvents. *J. Chem. Eng. Data* **2014**, *59*, 3652–3662.

(40) Chaumont, A.; Engler, E.; Schurhammer, R. Is charge scaling really mandatory when developing fixed charge atomistic force fields for deep eutectic solvents? *J. Phys. Chem. B* **2020**, *124*, 7239–7250.

(41) Kaur, S.; Shobhna,; Kashyap, H. K. Insights gained from refined force-field for pure and aqueous ethylene glycol through molecular dynamics simulations. *J. Phys. Chem. B* **2019**, *123*, 6543–6553.

(42) Kaur, S.; Malik, A.; Kashyap, H. K. Anatomy of microscopic structure of Ethaline deep eutectic solvent decoded through molecular dynamics simulations. *J. Phys. Chem. B* **2019**, *123*, 8291–8299.

(43) Mainberger, S.; Kindlein, M.; Bezold, F.; Elts, E.; Minceva, M.; Briesen, H. Deep eutectic solvent formation: a structural view using molecular dynamics simulations with classical force fields. *Mol. Phys.* **2017**, *115*, 1309–1321.

(44) Zhong, X.; Velez, C.; Acevedo, O. Partial charges optimized by genetic algorithms for deep eutectic solvent simulations. *J. Chen. Theory Comput.* **2021**, *17*, 3078–3087.

(45) Plimpton, S. Fast Parallel Algorithms for Short-range Molecular Dynamics. *J. Comput. Phys.* **1995**, *117*, 1–19.

(46) Hockney, R.; Eastwood, J. *Computer simulation using particles*; Adam Hilger, New York, 1989.

(47) Sun, H. COMPASS: An ab Initio Force-Field Optimized for Condensed-Phase ApplicationssOverview with Details on Alkane and Benzene Compounds. *J. Phys. Chem. B* **1998**, *102*, 7338–7364.

(48) Martinez, J. M.; Martinez, L. Packing Optimization for Automated Generation of Complex System's Initial Configurations for Molecular Dynamics and Docking. *J. Comput. Chem.* **2003**, *24*, 819–825.

(49) Martinez, L.; Andrade, R.; Martinez, J. M. Software News and Update Packmol: A Package for Building Initial Configurations for Molecular Dynamics Simulations. *J. Comput. Chem.* **2009**, *30*, 2157–2164.

(50) Hoover, W. G. Canonical Dynamics: Equilibrium Phase-space Distributions. *Phys. Rev. A* **1985**, *31*, 1695–1697.

(51) Shinoda, W.; Shiga, M.; Mikami, M. Rapid Estimation of Elastic Constants by Molecular Dynamics Simulation under Constant Stress. *Phys. Rev. B* **2004**, *69*, 134103.

(52) Zhang, Y.; Otani, A.; Maginn, E. J. Reliable Viscosity Calculation from Equilibrium

Molecular Dynamics Simulations: A Time Decomposition Method. *J. Chem. Theory Comput.* **2015**, *11*, 3537–3546.

(53) Zhang, Y.; Zhang, Y.; McCready, M. J.; Maginn, E. J. Evaluation and refinement of the general AMBER Force Field for nineteen pure organic electrolyte solvents. *J. Chem. Eng. Data* **2018**, *63*, 3488–3502.

(54) Yeh, I.; Hummer, G. System-size dependence of diffusion coefficients and viscosities from molecular dynamics simulations with periodic boundary condictions. *J. Phys. Chem. B* **2004**, *108*, 15873–15879.

(55) Moultos, O. A.; Zhang, Y.; Tsimpanogiannis, I. N.; Economou, I. G.; Maginn, E. J. System-size corrections for self-diffusion coefficients calculated from molecular dynamics simulations: The case of CO_2, n-alhanes, and poly(ethylene glycol) dimethyl ethers. *J. Chem. Phys.* **2016**, *145*, 074109.

(56) Lide, D. R., Ed. *CRC handbook of chemistry and physics, Internet Version 2005, http://www.hbcpnetbase.com*; CRC Press, Boca Raton, FL, 2005.

(57) Szefczyk, B.; Cordeiro, M. N. D. Physical properties at the base for the development of an all-atom force field for ethylene glycol. *J. Phys. Chem. B* **2011**, *115*, 3013–3019.

(58) D'Agostino, C.; Harris, R. C.; Abbott, A. P.; Gladden, L. F.; Mantle, M. D. Molecular motion and ion diffusion in choline chloride based deep eutectic solvents studied by 1H pulsed field gradient NMR spectroscopy. *Phys. Chem. Chem. Phys.* **2011**, *13*, 21383–21391.

(59) Kashyap, H. K.; Annapureddy, H. V.; Raineri, F. O.; Margulis, C. J. How is charge transport different in ionic liquids and electrolyte solutions? *J. Phys. Chem. B* **2011**, *115*, 13212–13221.

(60) Roy, S. et al. Structure and dynamics of the molten alkali-chloride salts from an X-ray, simulation, and rate theory persective. *Phys. Chem. Chem. Phys.* **2020**, *22*, 22900.

(61) Zhang, Y.; Maginn, E. J. Water-in-salt LiTFSI aqueous electrolytes (2): transport properties and Li^+ dynamics based on molecular dynamics simulations. *J. Phys. Chem. B* **2021**, Submitted.

Graphical TOC Entry